Supporting Information

Polyoxometalate-modified magnetic nanocomposite: A promising antibacterial material for water treatment

Yan Fang, Cuili Xing, Shixia Zhan, Meng Zhao, Mingxue Li*, Hongling Liu*

Henan Key Laboratory of Polyoxometalates, Institute of Molecular and Crystal Engineering, College of Chemistry and Chemical Engineering, Henan University, Kaifeng 475004, PR China

**E-mail: limingxue@henu.edu.cn(M.-X. Li);*

hlliu@henu.edu.cn (H.L.Liu)

Contents

1. Experimental section

1.1 Chemicals and Materials

Ferric chloride hexahydrate ($FeCl_3 \cdot 6H_2O$), sodium acrylate (Na acrylate), sodium acetate (NaOAc), ethylene glycol (EG), dopamine hydrochloride (DA) and trihydroxymethyl aminomethane (Tris) were obtained from Aldrich. Copper(II) perchlorate hexahydrate ($Cu(ClO_4)_2 \cdot 6H_2O$, 98%), 2-aminopyridine ($C_5H_6N_2$), sodium molybdate dihydrate ($Na_2MoO_4 \cdot 2H_2O$, 99%) and phosphoric acid (H_3PO_4, 85%) were purchased from J&K Scientific Ltd. Ni foams (99.8% purity, 0.5 mm thickness, 110 PPI pore size) were purchased from Yilongsheng energy technology co., Ltd. (Jiangsu, PR China). All chemicals were analytical grade and used without further purification. Deionized water was used for all synthetic processes.

1.2 Characterization

The microstructure and grain size of the nanoparticles were obtained by X-ray diffraction patterns (XRD, Philips X'Pert Pro, Philips, Amsterdam, Netherlands; λ = 1.54056Å) equipped with Cu *K*α radiation, transmission electron microscopy (TEM, FEI Tencnai G2 F30) and scanning electron microscopy images (SEM, Zeiss supra55). X-ray photoelectron spectroscopy (XPS) data were acquired on a scanning X-ray microprobe (Escalab 250xi) with Al Kα radiation as the excitation source. ICP analysis was performed using PerkinElemer (Optima 2100DV) machine to analyse copper (Cu) and molybdenum (Mo) concentration arising from POM in the sample. Elemental analyses (C, H and N) were investigated on a Perkin-Elmer 240 analyzer. The Fourier transform infrared (FT-IR) spectra were recorded with the wavelength range of 500–4000 cm^{-1} using an Avatar 360 FTIR spectrometer (FTIR, Nicolet Company, USA). The magnetic properties were subsequently investigated by a vibrating sample magnetometry (VSM, Lakeshore 7300). Zeta potential measurements were carried out in deionized water (pH 7.0) with a ZETASIZER Nano ZS instrument. The morphological changes of bacteria were monitored using SEM micrographs (Gemini 500). The UV–Vis absorption spectrum was recorded with a TU–1900 spectrometer (Beijing Purkinje General Instrument Co., Ltd., Beijing, China) at room temperature.

1.3 Preparation of POM

An methanol solution containing $Cu(ClO_4)_2 \cdot 6H_2O$ (0.056 g, 0.15 mmol) and 2-aminopyridine (0.028 g, 0.3 mmol) was stirred at 50 °C for 30 min. After cooling to room temperature, the solution was added to a 10 mL aqueous solution of $Na_2MoO_4 \cdot 2H_2O$ (0.145 g, 0.6 mmol), the pH value was maintained at 3.0 by dropwise addition of concentrated H_3PO_4 under continuous stirring. Then the mixture was stirred for 30 min and then filtered. The filtrate was placed at room temperature for slow evaporation. Blue crystals suitable for X-ray studies were obtained after 3 days. Yield: approx. 59% (based on Cu). Elemental analysis for $C_{40}H_{56}Cu_2Mo_{10}N_{16}O_{54}P_4$: calcd. C 16.90, H 1.92, N 7.89, Mo 33.83, Cu 4.48; Found: C 16.94, H 1.99, N 7.90, Mo 33.80, Cu 4.42. IR (KBr, cm^{-1}): 3324 (m), 3100 (w), 1660 (s), 1628 (s), 1543 (m), 1480 (m), 1421 (w), 1378 (m), 1328 (m), 1251 (w), 1168 (m), 1094 (s), 1032 (s), 915 (s), 898 (s), 786 (w), 694 (s), 585 (w).

1.4 Preparation of nickel foam

The pristine nickel foam was disposed according to the previous report by an optimized facile one-step hydrothermal method. $Ni(OH)_2$ hexagonal platelets were fabricated with sharp edges and high density.[1]

1.5 X-ray crystallography

A Siemens SMART-CCD diffractometer with graphite-monochromated MoKα radiation (λ = 0.71073 Å) was applied to collect the crystallographic data. The crystal structures of these complexes were solved through direct methods and refined by full-matrix least squares on F^2 with anisotropic displacement parameters for all non-hydrogen atoms using SHELXTL.[2] All hydrogen atoms were fixed at idealized geometrical positions. The crystallographic data, experimental details, and refinement results are summarized in Table S2. CCDC 1861727 contains the supplementary crystallographic data for this paper. These data can be obtained free of charge from The Cambridge Crystallographic Data Centre.

2. Supplementary characterization

The crystal structure of Standberg-type POM was shown in Fig. S1. The successful synthesis of POM was confirmed by FT-IR and PXRD characterizations (Fig. S2). The POM shows characteristic peaks of the $[P_2Mo_5O_{23}]^{6-}$ polyoxoanion: the peaks at 1093 cm^{-1}, 1032 cm^{-1} and 898 cm^{-1} are attributed to ν(P–O) and ν(Mo=O_d) stretching vibration, respectively.[3,4] These results are in good accordance with those of the X-ray diffraction structural analysis. PXRD spectra of as-prepared POM match well with the simulated pattern.

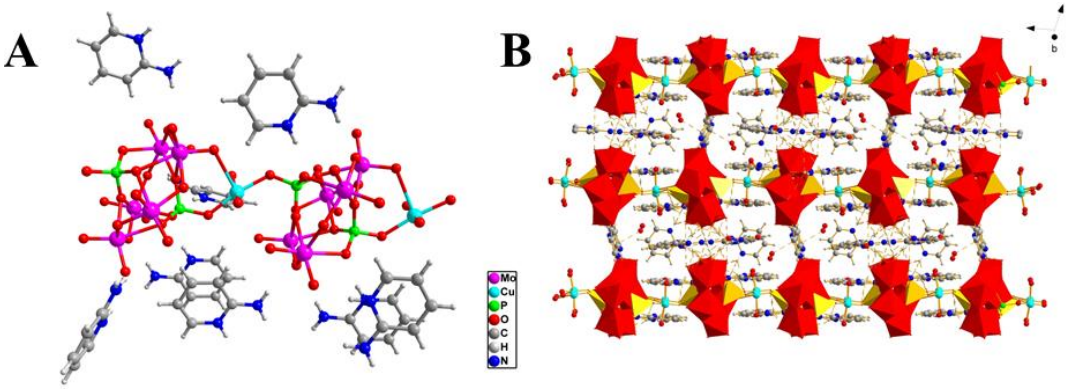

Fig. S1. (A) Crystal structure of POM, (B) Molecular packing projected.

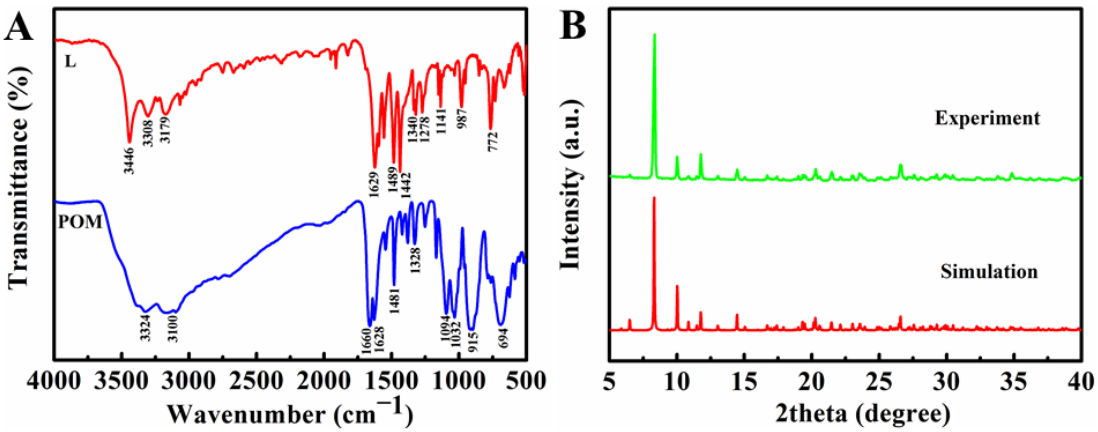

Fig. S2. (A) FT-TR spectra, (B) PXRD pattern of Standberg-type POM.

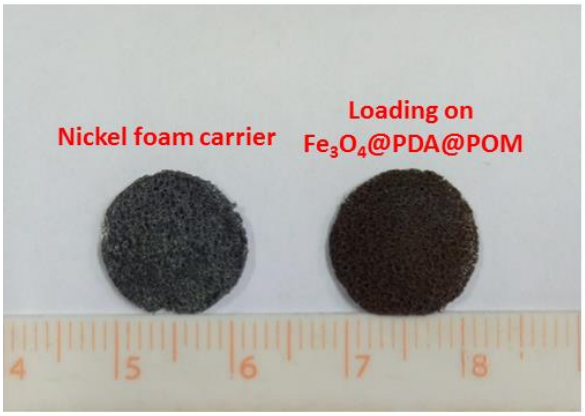

Fig. S3. Optical images of surface pretreated nickel foam (left) and Fe_3O_4@PDA@POM modified nickel foam (right).

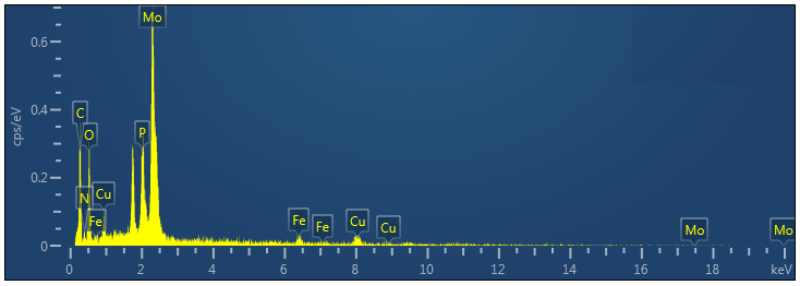

Fig. S4. EDX spectrum of the Fe_3O_4@PDA@POM nanocomposite.

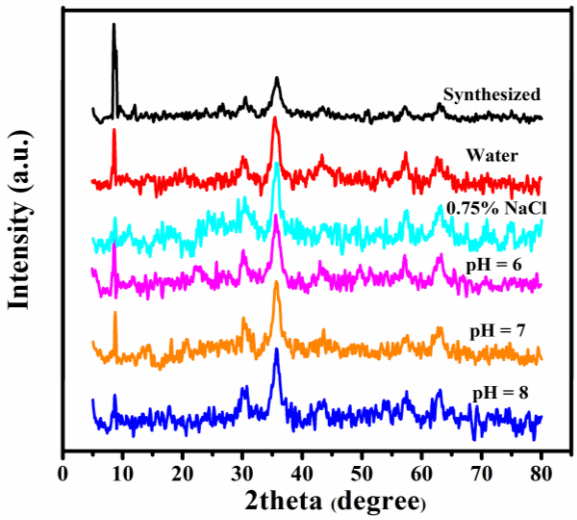

Fig. S5. The PXRD analysis of Fe_3O_4@PDA@POM nanocomposite in different solution (physiological buffers with pH of 6~8, 0.75% NaCl solution, and water) after 12 h dispersal.

Fig. S6. Nickel foam as the schematic diagram of filter membrane, with asepsis injector as reaction vessel.

Table S1. The application status of several surface modified Fe_3O_4@PDA nanocomposite.

Nanocomposites	**Surface modifier**	**Reaction conditions**	**Applications**	**Ref**
Fe_3O_4-HGNPs-Ab_2	Hollow gold nanoparticles; Antibody	Stirred	Determination of human IgG	5
Fe_3O_4@PDA/Au/PDA/Au/PDA	$HAuCl_4$	Aqueous solution	Catalyze the p-nitrophenol	6
MF@Fe_3O_4@PDA/PSBMA	Multifunctional melamine foam; Poly(sulfobetaine methacrylate)	Stirring	Aeparate oil/water mixtures and cationic-dye	7

Fe_3O_4@PDA@Ag	Ammonia silver solution	Ammonia silver solution	Organic dyes removal	8,9
Fe_3O_4@PDA@UiO-66-NH_2	UiO-66-NH_2	Heat, 140 ℃	Extract polychlorinated biphenyls; Enrichment of glycopeptides and phosphopeptides	10,11
Fe_3O_4@PDA@ZIF-8	Zeolitic imidazolate frameworks	Ultrasonication	Extract low-abundance peptides	12
Fe_3O_4@PDA-SO_3H	Sulfonic acid	Stirring	The formylation of alcohols and amines	13

Table S2. Crystal data and structure refinement results for POM.

Crystal Data	
Empirical formula	$C_{40}H_{56}Cu_2Mo_{10}N_{16}O_{54}P_4$
Formula weight	2835.37
crystal system	Triclinic
space group	*P-1*
Temperature (K)	296(2)
a (Å)	18.1100(11)
b (Å)	21.2840(13)
c (Å)	21.7984(14)
α (deg)	90.00
β (deg)	103.2850(10)
γ (deg)	90.00
Volume ($Å^3$)	8177.4(9)
Z	4
Calculated density (g cm^{-3})	2.303
Crystal size (mm^3)	0.28×0.23×0.14
Theta range for data collection (deg)	1.50–25.00
F(000)	5512
Limiting indices	$-21 \le h \le 21$, $-17 \le k \le 25$, $-25 \le l \le 25$
R_{int}	0.0252
parameters	1060
Reflections collected / unique	14320/11807
Final R indices [$I \ge 2\sigma(I)$]	$R_1 = 0.0383$, $wR_2 = 0.1023$
R indices (all data)	$R_1 = 0.0499$, $wR_2 = 0.1086$
Largest diff. peak and hole (e $Å^{-3}$)	2.526, − 2.050

Table S3. Metal element contents of the Fe_3O_4@PDA@POM nanocomposite based on ICP measurement.

	Element contents (wt%)		
Samples	Fe	Mo	Cu
Fe_3O_4@PDA@POM	29.98	6.28	1.05

Table S4. The control antibacterial studies against *E. coli*, $[P_2Mo_5O_{23}]^{6-}$, Cu^{2+} and L were assayed as the control.

	Samples Name					
	POM			L	Cu^{2+}	$[P_2Mo_5O_{23}]^{6-}$
Amounts (μmol)	0.1	0.2	0.5	2.6	0.6	0.5
Corresponding bacterial cell death (%)	55.9	79.8	91.6	17.0	58.2	49.5

Cu^{2+} derived from $Cu(ClO_4)_2 \cdot 6H_2O$ (M=370.53 g mol^{-1}); $[P_2Mo_5O_{23}]^{6-}$ derived from $(NH_4)_6[P_2Mo_5O_{23}]$ (M=997.70 g mol^{-1}).

Table S5. The antibacterial performance comparisons of the Fe_3O_4 coating nanocomposites already reported.

Materials	**Bacteria**	**Size (nm)**	**Antibacterial activity**	**Advantages**	**Ref.**
Graphene–Fe_3O_4	*E. coli*	200~250	74% (24 h)	Facile, suitable for water purification	14
Fe_3O_4@PDA@PAMAM@NONOate	*E. coli, S. aureus*	262	38%, 40% (20min)	Facile, easy recovery	15
Fe_3O_4/Ag@NFC	*S. aureus*	20~30	—	Facile, environmentally friendly, recyclable, suitable for medical and environmental applications	16
Fe_3O_4@CdS	*E. coli, S. saprophyticus*	14.2 ± 0.20	MIC = 5.0, 4.0 mg/mL (24h)	High effective, stability, reusability, suitable for environmental remediation	17
GO/Fe_3O_4/NPVP/Ag	*E. coli, S. aureus*	20~50	MIC = 31.25, 62.5 μg/mL (24h)	Effective, low cytotoxicity, suitable for medical care and food packaging	18
Fe_3O_4/Cu	*S. aureus, Bacillus Subtilis, E.coli*	62	MIC = 0.01, 0.04, 0.03 mg/ml	Facile, environmental compatibility	19
g-Fe_3O_4/2RGO	*Staphylococcus aureous, Bacillus subtilis, E. coli*	22 ± 2	MIC = 16, 10, 11.2 mg/mL	Good separation, easy recovery, suitable for pharmaceuticals and biomedical sectors	20
Fe_3O_4@PDA@POM	*E. coli, S. aureus*	340	99.9%, 99.9% (15 min)	Facile, high effective, recyclable, suitable for water treatment	This paper

3. Notes and references

1 L. J. Li, J. Xu, J. L. Lei, J. Zhang, F. McLarnon, Z. D. Wei, N. B. Li and F. S. Pan, *J. Mater. Chem. A,* 2015, **3,** 1953–1960.

2 G. M. Sheldrick, SHELXTL, Software Reference Manual, version 5.1; Bruker Analytical X-ray Instruments Inc: Madison; WI, 1997.

3 T. X. Wei, Y. Y. Chen, W. W. Tu, Y. Q. Lan and Z. H. Dai, *Chem. Commun.,* 2014, **50,** 9357–9360.

4 Y. M. Ji, C. G. Ma, J. Li, H. Y. Zhao, Q. Q. Chen, M. X. Li and H. L. Liu, *Nanomaterials,* 2018, **8,** 710–722.

5 Q. Wu, Y. Sun, D. Zhang, S. Li, X. H. Wang and D. Q. Song, *Biosens. Bioelectron.,* 2016, **86,** 95–101.

6 J. F. Zhang, Q. L. Fang, J. Y. Duan, H. M. Xu, H. J. Xu and S. H. Xuan, *Langmuir,* 2018, **34,** 4298–4306.

7 Y. Q. Zhang, X. B. Yang, Z. X. Wang, J. Long and L. Shao, *J. Mater. Chem. A,* 2017, **5,** 7316–7325.

8 K. X. Cui, B. Yan, Y. J. Xie, H. Qian, X. G. Wang, Q. X. Huang, Y. H. He, S. M. Jin and H. B. Zeng, *J. Hazard. Mater.,* 2018, **350,** 66–75.

9 Y. J. Xie, B. Yan, H. L. Xu, J. Chen, Q. X. Liu, Y. H. Deng and H. B. Zeng, *ACS Appl. Mater. Inter.,* 2014, **6,** 8845–8852.

10 S. C. Lin, N. Gan, Y. T. Cao, Y. J. Chen and Q. L. Jiang, *J. Chromatogr., A,* 2016, **1446,** 34–40.

11 Y. Q. Xie and C. H. Deng, *Sci. Rep.,* 2017, **7,** 1162–1169.

12 M. Zhao, Y. Q. Xie, H. M. Chen and C. H. Deng, *Talanta,* 2017, **167,** 392–397.

13 S. Taheri, H. Veisi and M. Hekmati, *New J. Chem.,* 2017, **41,** 5075–5081.

14 C. Santhosh, P. Kollu, S. Doshi, M. Sharma, D. Bahadur, M. T. Vanchinathan, P. Saravanan, B. S. Kim and A. N. Grace, *RSC Adv.,* 2014, **4,** 28300–28308.

15 S. M. Yu, G. W. Li, R. Liu, D. Ma and W. Xue, *Adv. Funct. Mater.,* 2018, **28,** 1707440.

16 R. Xiong, C. H. Lu, Y. R. Wang, Z. H. Zhou and X. X. Zhang, *J. Mater. Chem. A,* 2013, **1,** 14910–14918.

17 A. Samadi-Maybodi, M. R. Shariati and A. H. Colagar, *ChemPlusChem,* 2018, **83,** 769–779.

18 Q. Li, C. Yong, W. Cao, X. Wang, L. Wang, J. Zhou and X. Xing, *J. Colloid Interface Sci.,* 2018, **511,** 285–295.

19 R. Heydari, M. F. Koudehi and S. M. Pourmortazav, *ChemistrySelect,* 2019, **4,** 531–535.

20 D. K. Padhi, T. K. Panigrahi, K. Parida, S. K. Singh and P. M. Mishra, *ACS Sustain. Chem. Eng.,* 2017, **5,** 10551–10562.